

## Research paper

Using *in situ* cosmogenic  $^{10}\text{Be}$ ,  $^{14}\text{C}$ , and  $^{26}\text{Al}$  to decipher the history of polythermal ice sheets on Baffin Island, Arctic CanadaJason P. Briner<sup>a,\*</sup>, Nathaniel A. Lifton<sup>b</sup>, Gifford H. Miller<sup>c</sup>, Kurt Refsnider<sup>d</sup>, Rebecca Anderson<sup>e</sup>, Robert Finkel<sup>f</sup><sup>a</sup> University at Buffalo, Department of Geology, 411 Cooke Hall, Buffalo, NY 14260, USA<sup>b</sup> Purdue University, Departments of Earth and Atmospheric Sciences and Physics, West Lafayette, IN 47907, USA<sup>c</sup> INSTAAR and Department of Geological Sciences, University of Colorado, Boulder, CO 80303, USA<sup>d</sup> Prescott College, 220 Grove Avenue, Prescott, AZ 86301, USA<sup>e</sup> Alliance for Climate Education, 360 22nd Street, Oakland, CA 94612, USA<sup>f</sup> Department of Earth and Planetary Sciences, University of California, Berkeley, CA 94720, USA

## ARTICLE INFO

## Article history:

Received 13 February 2012

Received in revised form

6 November 2012

Accepted 7 November 2012

Available online 27 November 2012

## Keywords:

Cosmogenic nuclide

Polythermal ice sheet

Baffin Island

*In situ*  $^{14}\text{C}$  $^{10}\text{Be}$  dating

## ABSTRACT

Constraining the timing of past ice-sheet change is important for assessing the cryospheric expression of climate change and improving our understanding of ice sheet dynamics. Geochronology used to construct past ice-sheet reconstructions, however, can be ineffective in polar environments where ice sheets were polythermal and left varying imprints on landscapes. Cosmogenic-nuclide exposure dating, for example, is especially hampered by the lack of ice-sheet erosion and resultant cosmogenic nuclide inheritance. Here, we apply *in situ* cosmogenic  $^{10}\text{Be}$ ,  $^{14}\text{C}$  and  $^{26}\text{Al}$  methods to decipher various elements of the Laurentide Ice Sheet history of north-central Baffin Island. A clearly defined erosion boundary across the landscape reveals the transition in basal ice-sheet conditions as ice flow became channelized into northern Baffin Island fiords.  $^{10}\text{Be}$  and  $^{26}\text{Al}$  concentrations indicate that the boundary represents a juxtaposition of sliding, erosive ice and cold-bedded ice that preserved ancient bedrock that has not been significantly impacted by the ice sheet in perhaps one to two million years. We combine  $^{10}\text{Be}$  measurements from ice-sculpted bedrock with measurements of *in situ*  $^{14}\text{C}$ , which has no inheritance due to its quick decay during ice-sheet cover, to determine the local timing of deglaciation. The average  $^{10}\text{Be}$  and *in situ*  $^{14}\text{C}$  ages for upland deglaciation in north-central Baffin Island are  $7.7 \pm 0.9$  and  $8.4 \pm 1.4$  ka, respectively. Finally, *in situ*  $^{14}\text{C}$  measurements from surfaces being uncovered by present-day retreat of small ice caps mantling uplands within the study area have concentrations too low to be compatible with continuous post-glacial exposure. These samples require shielding by ice for a significant portion of the Holocene, and more burial than during the Little Ice Age alone. Simple exposure-burial modeling suggests that 2400–2900 yr of total ice cover during Neoglaciation is required to explain measured *in situ*  $^{14}\text{C}$  inventories. Combined, multiple cosmogenic nuclides with varying half-lives can be used to decipher many aspects of the history in landscapes occupied by polythermal ice sheets.

© 2012 Elsevier B.V. All rights reserved.

## 1. Introduction

Cosmogenic-nuclide exposure dating has emerged as a premiere tool for reconstructing glacier and ice sheet change (Balco, 2011). Users who first applied cosmogenic-nuclide exposure dating in high latitudes quickly realized that pervasive cosmogenic-nuclide inheritance (cosmogenic isotopes accumulated during

prior periods of exposure; henceforth termed “inheritance”) is a significant complication (e.g., Brook et al., 1993, 1996; Marsella et al., 2000). Yet, several workers used inheritance to their advantage by making inferences about ice-sheet erosion, and hence, the nature of past ice-sheet basal thermal regimes and dynamics (e.g., Fabel et al., 2002; Stroeven et al., 2002; Briner et al., 2003, 2005; Marquette et al., 2004; Staiger et al., 2006). The disequilibrium of  $^{26}\text{Al}$  and  $^{10}\text{Be}$  in rock samples with inheritance was also used to model the history of ice-sheet occupation over long timescales (100 ky to My; e.g., Bierman et al., 1999; Stroeven et al., 2002; Sugden et al., 2005; Li et al., 2008). Combined, these relatively recent applications of cosmogenic nuclides in polar landscapes

\* Corresponding author. Tel./Fax: +1 716 645 6800.

E-mail address: [jbriner@buffalo.edu](mailto:jbriner@buffalo.edu) (J.P. Briner).

have contributed to tremendous progress in our knowledge of ice-sheet history and dynamics.

Despite this progress, there remain limitations to using cosmogenic-nuclide exposure dating in landscapes covered by polythermal ice sheets. First, it is difficult to date the last deglaciation in these landscapes, although avoiding bedrock and dating erratics has proven successful in some instances (Stone et al., 2003; Håkansson et al., 2007; Goehring et al., 2008; Stroeven et al., 2011). However, terrain with pervasive inheritance commonly yields erratics with inheritance, and thus cosmogenic-nuclide exposure ages of erratics do not always chronicle the timing of deglaciation. Second, given the relatively long half-lives of  $^{26}\text{Al}$  and  $^{10}\text{Be}$  (~0.7 and 1.4 My, respectively), their ratio is unable to resolve whether burial occurred within the last glaciation (post-Marine Isotope Stage 5e) or earlier (Steig et al., 1998; Bierman et al., 1999; Fabel and Harbor, 1999). Thus, without an independent source of information about the presence or absence of past ice cover,  $^{26}\text{Al}$  and  $^{10}\text{Be}$  measurements alone may not reveal whether or not a landscape was occupied by non-erosive ice during the last glaciation.

*In situ*  $^{14}\text{C}$ , with its relatively short half-life (5730 years), enables one to circumvent the issues discussed above (Lifton et al., 2001). For example, while cover by non-erosive ice may not remove  $^{10}\text{Be}$  or  $^{26}\text{Al}$  from a landscape surface, *in situ*  $^{14}\text{C}$  will decay to background levels when a surface is occupied by non-erosive ice for intervals longer than ~30 ky. Therefore, the occupation of landscapes by non-erosive ice can be detected simply with measurements of *in situ*  $^{14}\text{C}$ . Miller et al. (2006) used *in situ*  $^{14}\text{C}$  measurements to determine deglaciation ages for summits in eastern Baffin Island and paired these *in situ*  $^{14}\text{C}$  ages with  $^{26}\text{Al}$  and  $^{10}\text{Be}$  measurements to place additional constraints on long-term ice sheet erosion. Following Miller et al. (2006), Anderson et al. (2008) measured *in situ*  $^{14}\text{C}$  in rock surfaces emerging from beneath small ice caps on uplands in north-central Baffin Island. The *in situ*  $^{14}\text{C}$  inventory, influenced by the shielding of late Holocene ice-cap occupation, allowed Anderson et al. (2008) to constrain the duration of late Holocene ice-cap cover. Here, we combine *in situ*  $^{14}\text{C}$  inventories with measurements of  $^{10}\text{Be}$  and  $^{26}\text{Al}$  to decipher the history of a landscape occupied by the polythermal northeastern Laurentide Ice Sheet (LIS). We add seven new *in situ*  $^{14}\text{C}$  measurements to six measurements published by Anderson et al. (2008) and combine these with 16 new  $^{10}\text{Be}$  and 2 new  $^{26}\text{Al}$  measurements. With this dataset we evaluate a major landscape boundary that separates non-eroded from ice-sculpted terrain in northern Baffin Island, which in turn allows us to assess the long-term pattern of LIS erosion. Furthermore, we provide additional age constraints on the timing of deglaciation and subsequent re-growth of small ice caps during the Holocene.

## 2. Study area

North-central Baffin Island consists of a broad, low relief upland that ranges in elevation from ~500–~800 m above sea level (asl) and hosts several small extant ice caps (Fig. 1). The upland is dissected by high-relief fiords along its northern and eastern margins, and gradually decreases in elevation into the Foxe Basin to the south and west. A visually well-defined landscape boundary separates terrain with obvious signs of glacial scouring to the north from terrain that lacks evidence of glacial scouring to the south (Fig. 2). The glacially scoured landscape consists of uneven terrain with exposed bedrock and with relief of up to 100s of meters and the presence of lakes; the non-scoured terrain has much lower relief, is covered by till, has rare outcrops of bedrock and the occasional meltwater channel, and has felsenmeer on mountain summits. Bedrock in this terrain is not glacially striated or polished, and includes various degrees of weathering of both bedrock outcrops and autochthonous blockfield (Fig. 3). The “erosion

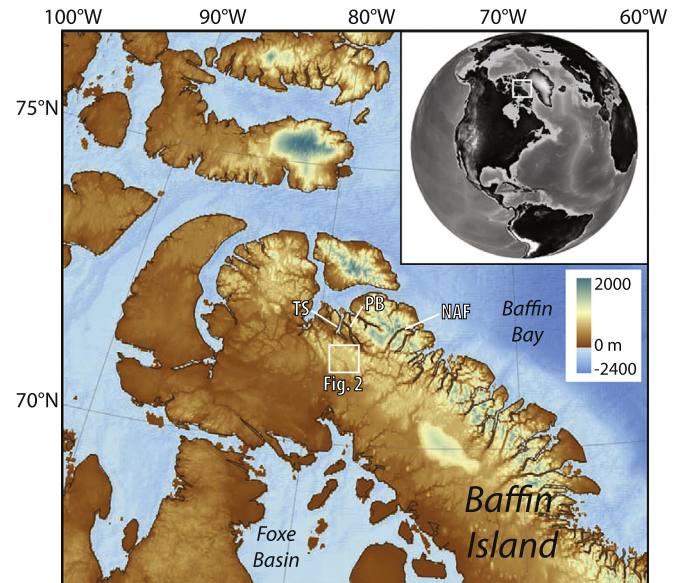
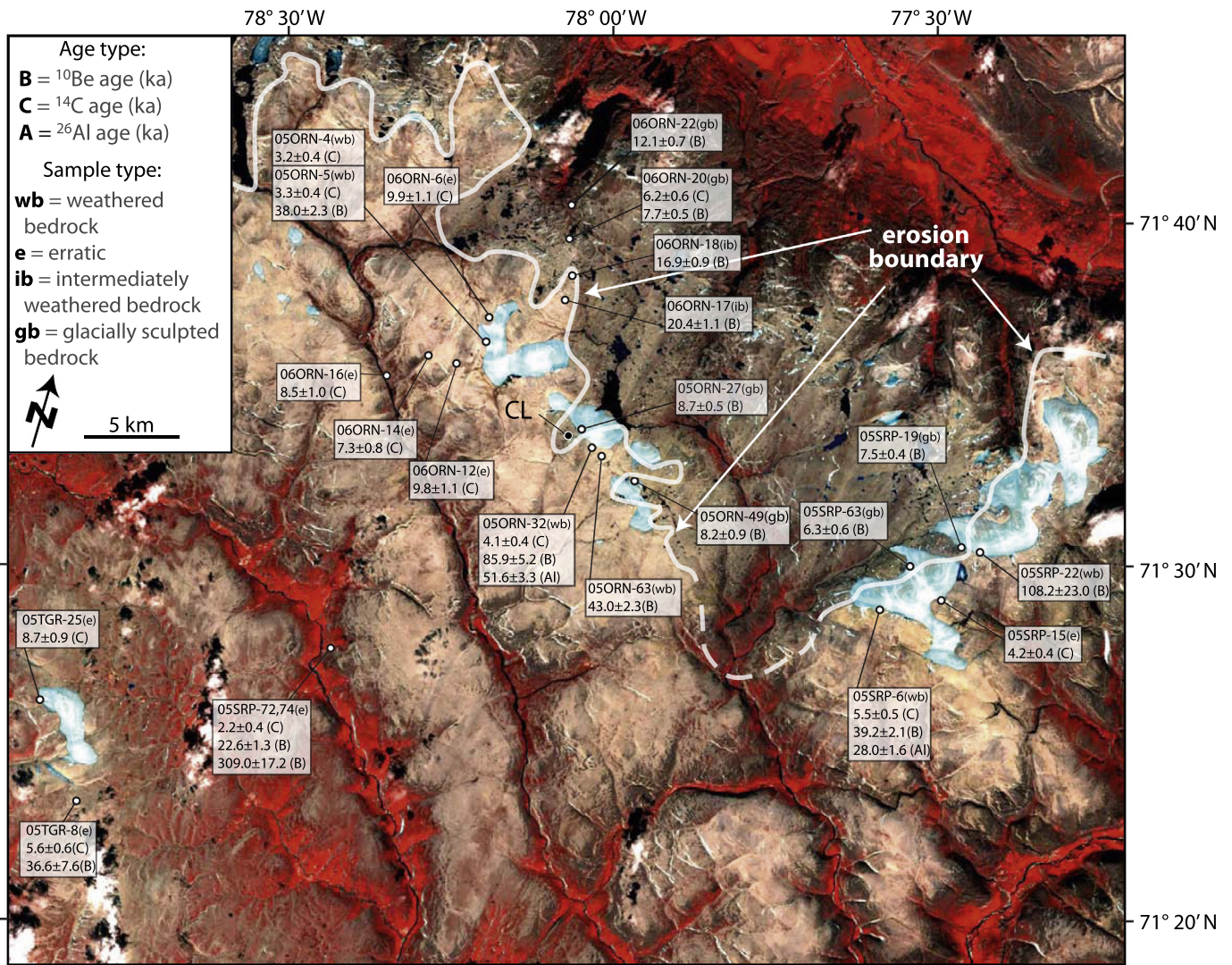


Fig. 1. Northern Baffin Island showing study area and context in northeastern North America (inset); TS = Tay Sound, PB = Paquet Bay, NAF = North Arm Fiord.

boundary” separating the two landscape zones runs irregularly across the northern side of the central Baffin uplands, and in our field area it separates the upland from the heads of valleys and fiords to the north. The elevation of the boundary varies and it does not seem to coincide with significant breaks in slope. The boundary is sharp in most locations, where ice-sculpted bedrock with straits appear a few 10s of meters from highly weathered bedrock; in some locations the transition from ice-sculpted bedrock to highly weathered bedrock spans hundreds of meters.

The glacial history of north-central Baffin Island has been the focus of a number of papers spanning the last half-century (e.g. Ives and Andrews, 1963; Falconer, 1966; Andrews and Barnett, 1979; Little et al., 2004; Utting et al., 2008; Refsnider and Miller, 2010). The LIS flowed northward and eastward across the plateau during the last glaciation, feeding ice streams that terminated in northern Baffin Bay (Dyke et al., 2003; De Angelis and Kleman, 2007). Staiger et al. (2006) measured  $^{10}\text{Be}$  and  $^{26}\text{Al}$  in till samples from northern Baffin Island and discovered a significant amount of cosmogenic nuclide inheritance in most of the high-elevation samples. This led Staiger et al. (2006) to show definitively that much of the upland escaped significant glacial scouring, as was previously hypothesized (Sugden, 1978; Andrews et al., 1985). Refsnider and Miller (2010) further support the antiquity of the north-central Baffin Island landscape by combining the cosmogenic radionuclide concentrations from Staiger et al. (2006) with till geochemistry measurements (Dredge, 2004; Utting et al., 2008) and burial/exposure modeling. The results reveal that till deposited on some parts of the north-Baffin landscape has been relatively immobile since 1.9–1.2 Ma, indicating at least minimally-erosive ice sheet conditions since that time.

Following the last glacial maximum, the LIS retreated from the continental shelf in northern Baffin Bay, through fiords, and eventually across north-central Baffin Island. Although recent research has focused on the timing of fiord deglaciation on southern (Marsella et al., 2000; Kaplan et al., 2001), eastern (Miller et al., 2002; Briner et al., 2007, 2009) and western Baffin Island (Dyke, 2008), there have not yet been any published detailed studies on the deglaciation of north-central Baffin Island. The deglaciation of eastern Baffin Island fiords typically occurred between 10 and 8 ka, followed by readvances in fiord heads ~8 ka (Andrews and Ives,



**Fig. 2.** Study region showing sample locations and erosion boundary. Brightly-toned areas are “lichen kill zones” produced by prolonged burial by snow and ice during the Little Ice Age. CL = Chisel Lake; base image is Landsat ETM+ acquired August 10, 2000.

1978; Dyke et al., 2003). The few radiocarbon ages from areas bordering the north Baffin plateau are consistent with this general pattern. Bivalves from raised marine deposits provide minimum ages of deglaciation of Tay Sound and Paquet Bay at  $7750 \pm 170$  cal yr BP (GSC-4317) and  $7200 \pm 215$  cal yr BP (GSC-4401), respectively (McNeely and Brennan, 2005). An additional

bivalve from raised marine deposits from inner North Arm Fjord is  $8460 \pm 170$  cal yr BP (GSC-6786; Little et al., 2004; McNeely and Brennan, 2005). Anderson et al. (2008) report an additional age constraint from the base of a lake sediment core from the center of the north Baffin plateau, indicating that the plateau was deglaciated before  $5630 \pm 25$  cal yr BP. Combined, the existing ages suggest that

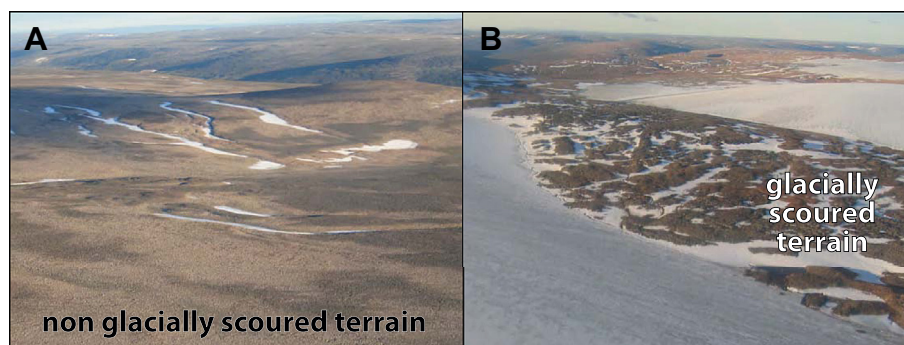


**Fig. 3.** Photographs of (A) weathered terrain found south of the erosion boundary, and (B) glacially eroded glacial terrain north of the erosion boundary. Note exposed bedrock and local relief in (A) and lack of bedrock outcrops and occasional meltwater channel in (B).

ice margins retreated onto the plateau ~8–7 ka, and entirely from the plateau before ~5.6 ka.

The north Baffin plateau today is occupied by a number of ice caps mantling the highest elevations. Brightly toned lichen-free landscapes surrounding these extant ice caps reveal that the ice caps and/or perennial snow areas were recently much more extensive (Ives, 1962; Andrews et al., 1976; Locke and Locke, 1977; Williams, 1978). The ongoing emergence of patterned ground and tundra vegetation from beneath the receding ice caps revealed that these ice caps are non-erosive and thus cold bedded, and radio-carbon “kill dates” from entombed surface vegetation reveal that the last phase of ice-cap expansion occurred during the Little Ice Age (Falconer, 1966). Building on Falconer (1966), Anderson et al. (2008) and Miller et al. (2012) provided hundreds of additional kill dates from several ice caps across the plateau, the temporal distribution of which reveals major expansion during the Little Ice Age. In addition, lake sediment cores and *in situ* <sup>14</sup>C analyses from recently exposed bedrock allowed Anderson et al. (2008) to suggest that ice caps were probably absent from the plateau during the millennia following deglaciation and are late Holocene features. The absolute timing of ice-cap growth is uncertain, although it likely took place after ~2800 cal yr BP and encompassed phases of ice-cap expansion prior to the Little Ice Age (Anderson et al., 2008).

### 3. Methods

We collected rock samples for <sup>26</sup>Al, <sup>14</sup>C and <sup>10</sup>Be measurements from north-central Baffin uplands in July 2005 (snow-free season) and April 2006 (snow-covered season). Our sampling strategy involved collecting samples from different landscape types (non-eroded vs. ice-sculpted) separated by a major landscape boundary, and collecting samples at varying distances and elevations in relation to the landscape boundary. Our strategy also involved the collection of both bedrock and erratic samples, and collecting samples at various distances from extant ice caps. Twenty-three rock samples were processed for <sup>26</sup>Al (*n* = 2), <sup>14</sup>C (*n* = 13) and <sup>10</sup>Be (*n* = 16). Both <sup>14</sup>C and <sup>10</sup>Be were measured in six samples, and all three isotopes were measured in two samples (Tables 1 and 2).

Samples were prepared for <sup>10</sup>Be and <sup>26</sup>Al measurement at the University at Buffalo following procedures modified from Kohl and Nishiizumi (1992). Isotope ratios were measured by accelerator mass spectrometry at the Center for Accelerator Mass Spectrometry (CAMS) at Lawrence Livermore National Laboratory. <sup>26</sup>Al/<sup>27</sup>Al ratios were compared to the <sup>26</sup>Al standard prepared by Nishiizumi (2004). <sup>10</sup>Be/<sup>9</sup>Be ratios for all but two samples were calculated using a recently revised ICN <sup>10</sup>Be standard (07KNSTD3110: <sup>10</sup>Be *t*<sub>1/2</sub> = 1.36 × 10<sup>6</sup> yr; Nishiizumi et al., 2007); 05SRP-72 & -74 were calculated using the previous standard at CAMS (KNSTD). <sup>10</sup>Be and <sup>26</sup>Al ratios of process blanks averaged 2.24 ± 0.45 × 10<sup>-14</sup> (*n* = 7) and 8.45 ± 8.1 × 10<sup>-15</sup> (*n* = 2), respectively. We calculated exposure ages using a modified version of the CRONUS-Earth online age calculator (Balco et al., 2008; <http://hess.ess.washington.edu/>) and the north-eastern North America <sup>10</sup>Be production rate (Balco et al., 2009), which includes a calibration site on Baffin Island. The modified calculator includes a higher-temporal-resolution geomagnetic field model (100-yr spacing vs. 500-yr) through the Holocene, which results in output that differs slightly from the online version – predictions from the two calculators agree within analytical uncertainties. The calculator has also been modified to allow calculation of *in situ* <sup>14</sup>C exposure ages. Sample position (latitude, longitude, elevation), topographic shielding and sample thickness were recorded in the field; samples were not adjusted for rock-surface erosion or seasonal snow shielding.

Samples for *in situ* <sup>14</sup>C concentration were prepared at the University of Arizona using methods modified from Lifton et al.

**Table 1**  
Sample information and <sup>10</sup>Be and <sup>26</sup>Al data.

Sample	Latitude (N)	Longitude (W)	Elevation (m asl)	Thickness (cm)	Shielding correction	Quartz (g)	Be carrier added (g)	<sup>10</sup> Be (atoms g <sup>-1</sup> yr)	<sup>10</sup> Be uncertainty (atoms g <sup>-1</sup> )	<sup>10</sup> Be age <sup>b</sup>	<sup>26</sup> Al (atoms g <sup>-1</sup> yr)	<sup>26</sup> Al uncertainty (atoms g <sup>-1</sup> )	<sup>26</sup> Al age <sup>b</sup>	<sup>26</sup> Al/ <sup>10</sup> Be
<i>North of the erosion boundary; glacially-sculpted bedrock</i>														
05ORN-27	71.5492	-78.0528	816	2.5	1.0	37.5404	0.3537	82268.2	2229.1	8.7 ± 0.5	NA	NA	NA	NA
05SRP-63	71.4909	-77.5534	759	4.5	1.0	40.9429	0.3510	55746.4	4176.1	6.3 ± 0.6	NA	NA	NA	NA
05ORN-49	71.5259	-77.9720	814	1.5	1.0	26.3793	0.3566	77915.4	7576.1	8.2 ± 0.9	NA	NA	NA	NA
06ORN-20	71.6370	-78.0894	760	1.0	1.0	40.4122	0.3142	69844.3	2588.1	7.7 ± 0.5	NA	NA	NA	NA
05SRP-19	71.4977	-77.4684	802	1.5	1.0	39.976	0.3438	70028.5	1932.3	7.5 ± 0.4	NA	NA	NA	NA
06ORN-22	71.6547	-78.0871	648	4.0	1.0	39.9822	0.3496	96146.2	2730.4	12.1 ± 0.7	NA	NA	NA	NA
<i>South of the erosion boundary, weathered bedrock</i>														
06-ORN-17	71.6114	-78.0831	806	1.0	1.0	40.2627	0.3568	192071.8	5021.3	20.4 ± 1.1	NA	NA	NA	NA
06-ORN-18	71.6207	-78.0765	816	6.0	1.0	40.8266	0.3507	153656.4	3395.6	16.8 ± 0.9	NA	NA	NA	NA
05ORN-32	71.5423	-78.0361	889	3.0	1.0	30.0447	0.3522	847028.5	29563.3	85.9 ± 5.2	3439454.7	132190.8	51.6 ± 3.3	4.06 ± 0.21
05SRP-22	71.4995	-77.4528	850	4.0	1.0	39.6685	0.3554	1014401.6	202880.3	108.2 ± 23.0	NA	NA	NA	NA
05ORN-5	71.5875	-78.1960	819	3.0	1.0	32.8918	0.3572	35022.7	12952.2	38.0 ± 2.3	NA	NA	NA	NA
06ORN-63	71.5393	-78.0274	880	2.5	1.0	40.5744	0.3312	423475.1	10424.9	43.0 ± 2.3	NA	NA	NA	NA
05SRP-6	71.3069	-77.5684	858	5.0	1.0	42.649	0.3544	373982.0	8832.8	39.2 ± 2.1	1804118.8	57998.5	28.0 ± 1.6	4.82 ± 0.19
<i>Erratics</i>														
05SRP-72	71.4458	-78.9761	451	5.0	1.0	28.3506	0.3779	158188.0	4940.3	22.6 ± 1.3	NA	NA	NA	NA
05SRP-74	71.4458	-78.9761	451	12.0	1.0	36.8858	0.3585	1951102.3	33332.2	309.0 ± 17.2	NA	NA	NA	NA
05TGR-8	71.3650	-78.7802	741	1.0	1.0	39.8981	0.3542	323194.9	64639.0	36.6 ± 7.6	NA	NA	NA	NA

NA = Not analyzed.

<sup>a</sup> All samples were spiked with a 1000 µg/g <sup>9</sup>Be carrier and AMS results are standardized to 07KNSTD3110 (except for 05SRP-72 & -74, standardized to KNSTD), a rock density of 2.65 g cm<sup>-3</sup>, and no post-glacial bedrock erosion and no snow cover.

<sup>b</sup> Be ages given in ka at 1SD using the Northeastern North America production rate and St scaling.

**Table 2**  
In-situ  $^{14}\text{C}$  data.

Sample	Latitude (N)	Longitude (W)	Elevation (m asl)	Thickness (cm)	Shielding correction	$^{14}\text{C}$ (atoms $\text{g}^{-1}$ )	$^{14}\text{C}$ uncertainty (atoms $\text{g}^{-1}$ )	$^{14}\text{C}$ age with St, Var atm, no geomag	$^{14}\text{C}$ age with Li w/geomag
<i>North of the erosion boundary; glacially-sculpted bedrock</i>									
06ORN-20	71.63700	-78.08940	760	1.0	1.0	144,954	8456	6.2 ± 0.6	6.2 ± 0.7
<i>South of the erosion boundary, weathered bedrock</i>									
05ORN-4	71.58749	-78.19596	819	5.0	1.0	89,189	8008	3.1 ± 0.4	3.1 ± 0.4
05ORN-5	71.58749	-78.19596	819	3.0	1.0	93,554	7988	3.3 ± 0.4	3.3 ± 0.4
05ORN-32	71.54229	-78.03614	889	3.0	1.0	118,798	8121	4.1 ± 0.4	4.1 ± 0.4
05SRP-6	71.30690	-77.56843	858	5.0	1.0	141,885	8099	5.5 ± 0.5	5.6 ± 0.5
<i>Erratics</i>									
05TGR-8	71.36500	-78.78017	741	1.0	1.0	132,315	8580	5.5 ± 0.6	5.6 ± 0.6
05TGR-25	71.40638	-78.82883	738	1.0	1.0	176,124	8267	8.7 ± 0.9	8.8 ± 1.0
06ORN-6	71.53653	-78.12423	769	8.0	1.0	184,068	8279	9.9 ± 1.1	10.0 ± 1.2
06ORN-12	71.58384	-78.26545	778	1.5	1.0	194,235	8286	9.8 ± 1.1	10.0 ± 1.1
06ORN-14	71.57642	-78.28785	716	1.0	1.0	156,232	8441	7.3 ± 0.8	7.4 ± 0.8
06ORN-16	71.57025	-78.35144	640	1.0	1.0	159,634	8493	8.5 ± 1.0	8.7 ± 1.0
05SRP-15	71.47530	-77.51290	797	4.0	1.0	110,342	8034	4.2 ± 0.4	4.2 ± 0.5
05SRP-72	71.44578	-78.97612	451	5.0	1.0	45,963	7762	2.2 ± 0.4	2.2 ± 0.4

Note: St and Li scaling schemes are described in Balco et al. (2008); Samples 05ORN-04, -05, -32, 05SRP-15, 05TGR-08 and 06ORN-20 were reported in Anderson et al. (2008). Ages calculated assuming SLHL spallogenic production rates of  $12.4 \pm 0.6$  atoms  $\text{g}^{-1} \text{y}^{-1}$  and  $13.6 \pm 0.6$  at  $\text{g}^{-1} \text{y}^{-1}$  for St and Li, respectively, derived based on analyses in Lifton et al. (2001), Miller et al. (2006) and Dugan, (2008) as described in the text. SLHL muogenic production rates taken from Heisinger et al. (2002a, b) following Balco et al. (2008).

(2001), Dugan (2008), Pigati (2004), and Miller et al. (2006). The extraction process involves combusting  $\sim 5$  g of quartz at  $500^\circ\text{C}$  for 1 h to remove atmospheric contaminants, followed by dissolution in a degassed  $\text{LiBO}_2$  flux at  $1100^\circ\text{C}$  for 3 h. Both steps take place in an atmosphere of 50 torr of Research Purity  $\text{O}_2$ . Any carbon species released during the high-temperature step are oxidized to  $\text{CO}_2$ , which is then purified, measured quantitatively, and converted to graphite for  $^{14}\text{C}$  measurement by accelerator mass spectrometry (Lifton et al., 2001). All *in situ*  $^{14}\text{C}$  ages have been calculated using the version of the Balco et al. (2008) calculator described above, with SLHL production rates derived from Lifton et al. (2001), Miller et al. (2006) and Dugan (2008) (Table 2). Weighted mean values of replicate calibration sample measurements from each study were calculated prior to, and used in, the production rate calculations to avoid undue weight being placed on the replicates.

Six of the *in situ*  $^{14}\text{C}$  ages reported here were also reported in Anderson et al. (2008); these have been updated (Table 2) to reflect more appropriate data reduction procedures. First, we switched to using the unweighted mean and standard deviation for our long-term blank values. These should be more representative of the distribution of blanks experienced by the sample measurements presented here. Second, we now calculate *in situ*  $^{14}\text{C}$  concentrations using the procedure of Hippe et al. (2013). We concur with Hippe et al.'s (in press) argument that since *in situ*  $^{14}\text{C}$  is inorganic and not affected by  $^{14}\text{C}$  produced via atmospheric thermonuclear testing in the 1950s, AMS measurements for *in situ*  $^{14}\text{C}$  do not require normalization to 1950 and -25 per mil PDB. Those two changes in our data reduction methods yield slightly different values from those previously published, yet the changes are insignificant at  $1\sigma$ .

#### 4. Cosmogenic nuclide results

Samples collected on both sides of the erosion boundary are from erratics ( $n = 9$ ), glacially sculpted bedrock ( $n = 6$ ) and weathered bedrock ( $n = 8$ ; Tables 1 and 2). Sample elevations range from  $\sim 450$ – $\sim 900$  m asl. Six samples (all bedrock) are from north of the erosion boundary in scoured terrain, and two samples were collected from bedrock in an area where the boundary is diffuse (06ORN-17, 06ORN-18; Fig. 2). Fifteen samples were collected south of the erosion boundary in unscoured terrain; nine from erratics and six from weathered bedrock and felsensmeer. All ages and sample IDs are shown in Fig. 2. All ages are reported with the

“St” scaling schemes of Balco et al. (2008); ages calculated with alternative scaling schemes are reported in supplemental Table 1.

##### 4.1. Erratics

We obtained three  $^{10}\text{Be}$  ages on erratics, all from the southwestern portion of the field area. Beryllium-10 ages from two erratic cobbles resting atop a sandy kame are  $22.6 \pm 1.3$  and  $309.0 \pm 17.2$  ka (05SRP-72 and 05SRP-74, respectively). A third erratic boulder has a  $^{10}\text{Be}$  age of  $36.6 \pm 7.6$  ka (05TGR-8). *In situ*  $^{14}\text{C}$  ages from two of these erratics are  $2.2 \pm 0.4$  ka (05SRP-72) and  $5.5 \pm 0.6$  ka (05TGR-8). We obtained *in situ*  $^{14}\text{C}$  ages on six additional erratic boulders. One erratic, also from the southwestern part of the study area, yields an *in situ*  $^{14}\text{C}$  age of  $8.7 \pm 0.9$  ka (05TGR-25). Five additional erratics, some near ice cap margins and some farther away, yield *in situ*  $^{14}\text{C}$  ages ranging from  $9.8 \pm 1.1$  ka (06ORN-12) to  $4.2 \pm 0.4$  ka (05SRP-15) (Table 2, Fig. 4).

##### 4.2. Ice-sculpted bedrock

We obtained  $^{10}\text{Be}$  ages from 6 different outcrops of glacially sculpted bedrock with visible striations and glacial polish, all north of the erosion boundary. Two samples from the headwaters of a valley incised into the plateau are  $12.1 \pm 0.7$  ka (06ORN-22) and  $7.7 \pm 0.5$  ka (06ORN-20; Fig. 4). Four additional samples are from near the erosion boundary in locations where there is a sharp break between ice-scoured and non-ice-scoured terrain. Two samples from the central part of the study area are  $8.7 \pm 0.5$  ka (05ORN-27) and  $8.2 \pm 0.9$  ka (05ORN-49). Two samples from the eastern part of the study area are  $7.5 \pm 0.4$  ka (05SRP-19) and  $6.3 \pm 0.6$  ka (05SRP-63). We obtained one *in situ*  $^{14}\text{C}$  age from ice-sculpted bedrock; sample 06ORN-20 yielded an age of  $6.2 \pm 0.6$  ka.

##### 4.3. Weathered bedrock

Seven  $^{10}\text{Be}$  ages are from weathered bedrock; these are apparent ages because of their complex exposure history, as suggested by measurements from  $^{26}\text{Al}$  and  $^{14}\text{C}$  in some of the samples (see below). Two samples are from an area where the erosion boundary is diffuse. The bedrock in this area is intermediately weathered; it is not frost-riven into blockfield and does not contain weathering pits, yet it lacks striations and an overall ice-sculpted profile. The apparent  $^{10}\text{Be}$  ages are  $16.9 \pm 0.9$  ka (06ORN-18) and  $20.4 \pm 1.1$  ka



**Fig. 4.** Photographs of samples collected in summer 2005 and spring 2006, illustrating different samples types found in the field area: (A) glacially sculpted bedrock, (B) erratic boulders, (C) frost-riven blockfield, and (D) weathered bedrock outcrops.

(06ORN-17). Three apparent  $^{10}\text{Be}$  ages from weathered bedrock near the ice caps in the central portion of the study area are  $85.9 \pm 5.2$  ka (05ORN-32),  $43.0 \pm 2.3$  ka (05ORN-63) and  $38.0 \pm 2.3$  ka (05ORN-5; Fig. 4). Two additional apparent  $^{10}\text{Be}$  ages from weathered bedrock near the ice caps in the eastern portion of the study area are  $39.2 \pm 2.1$  ka (05SRP-6; Fig. 4) and  $108.2 \pm 23.0$  ka (05SRP-22).  $^{26}\text{Al}$  measurements on two of these samples yielded ages of  $51.6 \pm 3.3$  ka (05ORN-32) and  $28.0 \pm 1.6$  ka (05SRP-6). The combined data from 05ORN-32 and 05SRP-6 yield  $^{26}\text{Al}/^{10}\text{Be}$  ratios of  $4.06 \pm 0.21$  and  $4.82 \pm 0.19$ , respectively. Finally, we obtained *in situ*  $^{14}\text{C}$  ages from these same two samples; 05ORN-32 yielded an age of  $4.1 \pm 0.4$  ka, and 05SRP-6 yielded an age of  $5.5 \pm 0.5$  ka. Two additional weathered bedrock samples yielded *in situ*  $^{14}\text{C}$  ages of  $3.1 \pm 0.4$  ka (05ORN-4) and  $3.3 \pm 0.4$  ka (05ORN-5); all four *in situ*  $^{14}\text{C}$  ages are from weathered bedrock within a few 10s of meters of ice-cap margins in 2005.

## 5. Interpretation and discussion

### 5.1. Be and Al ages and the erosion boundary

The boundary separating the fiord landscape of northeastern Baffin Island from the north-central uplands subdivides the Baffin Island landscape into regions of selective linear erosion and those with little to no signs of glacial erosion outlined by Sugden (1978). Our  $^{10}\text{Be}$  ages from bedrock north of the erosion boundary provide ages consistent with the timing of deglaciation in almost all cases, suggesting that sufficient glacial erosion ( $\sim 2$  m) has taken place to remove cosmogenic nuclide inventories acquired during prior periods of exposure (i.e., prior interglaciations). This is consistent with significant glacial scouring of bedrock surfaces observed in the field.

The young  $^{10}\text{Be}$  ages north of the erosion boundary contrast with apparent  $^{10}\text{Be}$  ages from south of the boundary that significantly pre-date the last deglaciation. The five apparent  $^{10}\text{Be}$  ages from weathered bedrock range from  $\sim 38$  to  $\sim 108$  ka. Furthermore,

the two samples with paired  $^{26}\text{Al}$  measurements, 05SRP-6 and 05ORN-32 (Fig. 5), yield minimum total histories of 760 ka and 1.15 Ma, respectively. These long histories are consistent with total histories calculated for till samples from the north-central Baffin Island plateau and uplands adjacent to fiord heads north of the plateau (Staiger et al., 2006; Refsnider and Miller, 2010). However, because these are minimum estimates, we would like to better constrain the total histories. Although an infinite number of combinations of exposure, burial, and erosion can explain the measured cosmogenic nuclide inventories of such samples, the nature of the cyclical glaciation-interglaciation (burial-exposure) histories of these samples limit the range of geologically reasonable scenarios. We explore such scenarios using a simple model in which a  $^{10}\text{Be}$ - $^{26}\text{Al}$  inventory developed during the Pliocene evolves through periods of burial and exposure corresponding to 41-ka glacial cyclicity until 1 Ma and 100-ka cyclicity subsequently; there is variable erosion during both interglaciations and glaciations (Fig. 5). Model parameters specific to cosmogenic nuclide systematics follow those used in the CRONUS-Earth online age calculator with St production rate scaling (Balco et al., 2008; <http://hess.ess.washington.edu/>). Cosmogenic nuclide production occurs in the model only during interglaciations.

Sample 05SRP-6 is from frost-riven bedrock that has been fractured *in situ* into boulders; quartz veins are discernable as linear arrays of quartz-rich boulders. Erratics are present in low abundances, but there is no evidence of past cover by till. Based on the modeling (Fig. 5), this site has experienced average exposure durations during interglaciations equivalent to 10% or less of its total history under a wide range of erosional scenarios. Sample 05ORN-32, which has higher  $^{26}\text{Al}/^{10}\text{Be}$  disequilibrium (lower ratio) than 05SRP-6, also most likely experienced average exposure durations of 5–10% during its total history. All reasonable model scenarios for both samples are inconsistent with appreciable erosion since  $\sim 1$  Ma and suggest average exposure during interglaciations comparable in duration to Holocene exposure at the sites. Sample 05SRP-6 likely experienced some glacial erosion

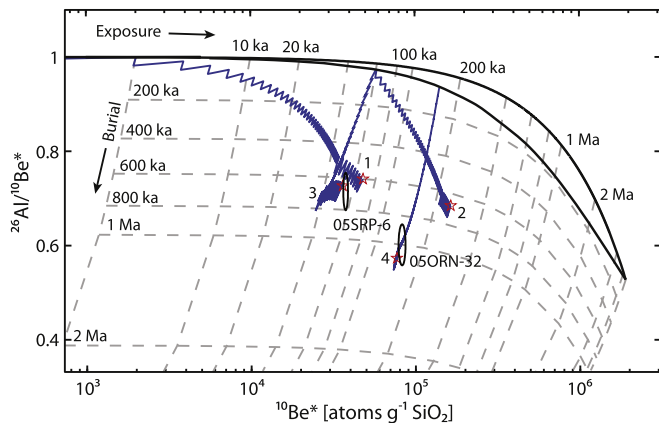


**Fig. 5.**  $^{10}\text{Be}$ - $^{26}\text{Al}$  two-nuclide evolution plot; ellipses show  $1\sigma$  analytical uncertainties of samples 05SRP-6 and 05ORN-32. The y-axis values are normalized to the  $^{26}\text{Al}/^{10}\text{Be}$  surface production ratio and the x-axis values are normalized to sea level-high latitude production rates. The solid black lines show the cosmogenic-nuclide inventories for no erosion (upper) and steady erosion (lower) scenarios. The gray dashed lines are burial and exposure isochrons. The sawtooth-shaped curves show the cosmogenic-nuclide evolution for a range of burial-exposure-erosion scenarios, each of which includes the onset of glacial-interglacial cycles at 2.7 Ma, 40 ky glacial cycles prior to 1 Ma, and 100 ky glacial cycles afterward. We display four scenarios with these variables:  $f$  is the percentage of each cycle that the sample remains buried by glacial ice,  $t_0$  is the duration of pre-glacial exposure,  $E_0$  is the pre-glacial erosion rate,  $E_{\text{interglacial}}$  is the erosion rate during interglaciations, and  $E_{\text{glacial}}$  is the amount of rock eroded per glaciation. (1) No inherited pre-glacial nuclide inventory:  $t_0 = 0$  Ma,  $E_0 = 0$  m/Ma,  $f = 95\%$ ,  $E_{\text{interglacial}} = 1$  m/Ma, and  $E_{\text{glacial}} = 0$  cm; (2) Inherited pre-glacial nuclide inventory:  $t_0 = 2.5$  Ma,  $E_0 = 15$  m/Ma,  $f = 85\%$ ,  $E_{\text{interglacial}} = 1$  m/Ma, and  $E_{\text{glacial}} = 0$  cm; (3) Inherited pre-glacial nuclide inventory with minor glacial erosion:  $t_0 = 2.5$  Ma,  $E_0 = 15$  m/Ma,  $f = 95\%$ ,  $E_{\text{interglacial}} = 1$  m/Ma, and  $E_{\text{glacial}} = 5$  cm; (4) Inherited pre-glacial nuclide inventory with moderate glacial erosion:  $t_0 = 2.5$  Ma,  $E_0 = 5$  m/Ma,  $f = 95\%$ ,  $E_{\text{interglacial}} = 1$  m/Ma, and  $E_{\text{glacial}} = 0$  cm.

during the Early Pleistocene, but sample 05ORN-32 may not have experienced any appreciable glacial erosion during the Pleistocene. Thus, the erosion boundary delimits the edge of a landscape with a long history of cover by predominantly cold-based ice during glaciations.

The width of the erosion boundary appears narrow in most places throughout the field area. In areas surrounding finger-like erosional zones that protrude southward into the non-eroded terrain, samples very close to each other have drastically different  $^{10}\text{Be}$  concentrations. For example, 05SRP-19 (802 m asl) provides a deglaciation age ( $7.5 \pm 0.4$  ka), and lies only 580 m from 05SRP-22 (850 m asl), which has an apparent  $^{10}\text{Be}$  age of  $108.2 \pm 23.0$  ka. In a second location, sample 05ORN-27 (816 m asl) yields a deglaciation age ( $8.7 \pm 0.5$  ka), yet 950 m away sample 05ORN-32 (889 m asl) yields an apparent  $^{10}\text{Be}$  age of  $85.9 \pm 5.2$  ka, and a paired-nuclide history of  $\sim 1.15$  Ma. In other areas, however, where the boundary is more diffuse, samples show a lower gradient in changing  $^{10}\text{Be}$  concentrations. For example, samples 06ORN-17 (806 m asl), 06ORN-18 (816 m asl) and 06ORN-20 (760 m asl) are aligned in a south-to-north transect and span intermediately weathered bedrock to ice-scoured bedrock. The apparent  $^{10}\text{Be}$  ages of  $20.4 \pm 1.1$  ka (06ORN-17),  $16.8 \pm 0.9$  ka (06ORN-18) and  $7.7 \pm 0.5$  ka (06ORN-20) reveal progressively decreasing amounts of inheritance, and increasing erosion, across the boundary. Although in general there is a relationship between inheritance and elevation (Fig. 6), this relationship is not consistent everywhere, which was also noted by Staiger et al. (2006).

There is ample evidence that broad areas of interior Baffin Island escaped significant glacial erosion because it has been occupied mostly by cold-bedded ice during Quaternary glaciations (e.g., Sugden, 1978; Andrews et al., 1985; Kleman and Hättestrand, 1999; Staiger et al., 2006; Refsnider and Miller, 2010). Observation-based

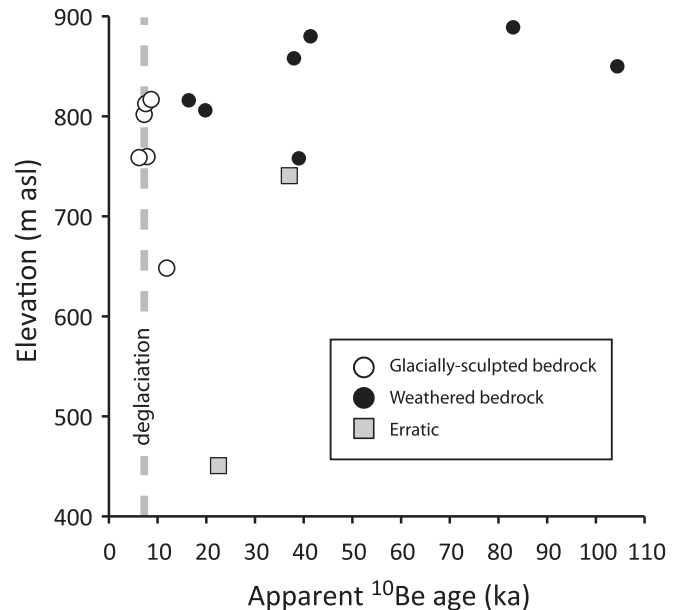


**Fig. 6.** Apparent  $^{10}\text{Be}$  age versus elevation showing pervasive inheritance in weathered bedrock and erratic samples.

arguments for a transition from cold-bedded to warm-bedded conditions where ice became channelized through topography as it neared the coast have been recently supported with cosmogenic nuclide data (e.g., Miller et al., 2002; Briner et al., 2006; Staiger et al., 2006). In Scandinavia, recent studies have discussed erosion boundaries far inland, and constrained their character and evolution using geomorphology and cosmogenic isotopes (e.g., Kleman, 1994; Fabel et al., 2002; Stroeven et al., 2002; Harbor et al., 2006). However, the location and character of the boundary on Baffin Island has received less attention. Along the eastern fiords of Baffin Island, Briner et al. (2008) used cosmogenic nuclides and the lake-density pattern to show that the zone of erosion extended well inland of the head of Clyde Inlet. There, the erosion boundary is defined by topography, much like within the fiord landscape, and thus fits the description of selective linear erosion (Sugden, 1978). The erosion boundary bordering the northern edge of the north-central Baffin, however, is not as easily explained by topography alone. We suggest that as ice flowed northward across the plateau (Little et al., 2004) and became channelized into the Tay Sound and Paquet Bay, convergent flow resulted in increased discharge, increased basal velocity, and the ice-sheet bed became temperate and sliding occurred (Kleman and Stroeven, 1997; Kleman et al., 2008).

The erosion boundary marks the edge of very ancient landscapes, implying that actively eroding ice was closely juxtaposed to cold-bedded ice during the last glacial cycle (Staiger et al., 2006). We think it is unlikely that the sharp erosion boundary created during the last glacial cycle was located in the same exact position during the numerous previous glaciations throughout the Quaternary, and we think it is incompatible with our results that the erosion boundary was farther inland prior to the last glaciation. Thus, we think it is more plausible that erosion took place farther inland during the last glacial cycle than during previous glaciations (Harbor et al., 2006). This could be due to thicker ice during the last glacial cycle leading to more ice focusing, and thus basal sliding occurring farther inland. Or, perhaps the landscape is continuously evolving, as implied by Refsnider and Miller (2010), who argued that ice piracy through the Quaternary has led to ice being progressively focused into some fiords more than others, a concept

that is also supported by modeling (Kessler et al., 2008). In either case, varying ice-sheet basal conditions, from till deposition early during the Quaternary, to subsequent cold-bedded conditions, to the inland migration of sliding ice during the last glacial cycle, indicates an evolution of ice-sheet behavior throughout the Quaternary.

### 5.2. The timing of deglaciation

Two groups of samples constrain the timing of deglaciation of the north-central Baffin upland:  $^{10}\text{Be}$  ages from ice-sculpted bedrock and the *in situ*  $^{14}\text{C}$  ages. All three  $^{10}\text{Be}$  ages from erratics pre-date the last deglaciation, and thus contain inheritance; this perhaps is not surprising given the antiquity of the tills mantling parts of the uplands that likely contain material recycled during multiple glaciations (Staiger et al., 2006). Of the six  $^{10}\text{Be}$  ages from sculpted bedrock, one sample likely contains inheritance (06ORN-22), because its apparent  $^{10}\text{Be}$  age ( $12.1 \pm 0.7$  ka) pre-dates radiocarbon ages of 7–8 cal ka BP from bivalves far downvalley. The remaining five samples have an average  $^{10}\text{Be}$  age of  $7.7 \pm 0.9$  ka. Anderson et al. (2008) reported two basal radiocarbon ages from a sediment core from Chisel Lake (informal name,  $71^{\circ}32'45''$  N,  $78^{\circ}93'50''$  W; Fig. 2) that average  $5.61 \pm 0.03$  cal ka, indicating deglaciation prior to this time. The  $^{10}\text{Be}$  age for deglaciation is older; this might either be due to a minor amount of inheritance influencing the  $^{10}\text{Be}$  ages, or perhaps the lowest material dated in the Chisel Lake core does not closely constrain the timing of deglaciation.

The *in situ*  $^{14}\text{C}$  ages span the Holocene, ranging from  $\sim 2$  to  $\sim 10$  ka. Many of the samples are consistent with deglaciation during the early Holocene, whereas others clearly post-date deglaciation. We interpret the youngest *in situ*  $^{14}\text{C}$  ages as having been partially shielded by ice caps that have periodically regrown over the plateau during the late Holocene (Anderson et al., 2008; see below). Given the location of the field site and the likelihood of its occupation by thick ice throughout the last glaciation, we consider it implausible that there is any inherited *in situ*  $^{14}\text{C}$ , and interpret the oldest *in situ*  $^{14}\text{C}$  ages to represent deglaciation. We consider the *in situ*  $^{14}\text{C}$  ages that are younger than the oldest radiocarbon ages from Chisel Lake as post-dating deglaciation. Taking an average of all *in situ*  $^{14}\text{C}$  ages statistically older than  $5.61 \pm 0.03$  cal ka yields an average *in situ*  $^{14}\text{C}$  age of  $8.4 \pm 1.4$  ka ( $n = 6$ ). This age is indistinguishable from the average  $^{10}\text{Be}$  age of  $7.7 \pm 0.9$  ka; thus, we consider the  $^{10}\text{Be}$  ages as not significantly influenced by inheritance (excluding 06ORN-22), and therefore they represent the likely timing of upland deglaciation. Combining  $^{10}\text{Be}$  and *in situ*  $^{14}\text{C}$  ages yields an average age for deglaciation of  $8.1 \pm 1.2$  ka.

Our age assignment for deglaciation ( $\sim 8$  ka) is statistically similar to the radiocarbon-dated marine sediments in the fiords north of the plateau, and is consistent with the broad pattern of retreat outlined by Dyke et al. (2003). On the other hand, Dyke (2008) suggests that ice was still  $\sim 1000$  m thick on the central Baffin Island ice divide  $\sim 7.4$  cal ka, and has reconstructed ice flow at lower elevations farther south of our study area as late as  $\sim 4.5$  cal ka. This very late ice flow even post-dates the basal radiocarbon ages from the Chisel Lake sediment core by  $\sim 1000$  yr. Combined, these datasets suggest that ice on central-Baffin Island retreated southward, towards the Barnes Ice Cap, throughout the Holocene. Furthermore, these data support Dyke et al. (2003) depiction that the northernmost uplands deglaciated first.

### 5.3. *In situ* $^{14}\text{C}$ and Neoglaciation

Another prominent boundary in the landscape of north-central Baffin Island is the vegetation trimline that delimits the extent of permanent snow and ice cover during the Little Ice Age (Ives, 1962;

Andrews et al., 1976; Locke and Locke, 1977; Willams, 1978). Anderson et al. (2008) demonstrated by radiocarbon dating preserved vegetation that was being exposed at retreating ice margins that major ice-cap expansion events occurred  $\sim 1250$  AD and  $\sim 1450$  AD. Thus, many of the  $^{10}\text{Be}$  and *in situ*  $^{14}\text{C}$  ages presented here, especially those within the vegetation trimline (Fig. 2), have been affected by at least  $\sim 500$ – $700$  years of snow shielding. Because of the relatively short  $^{14}\text{C}$  half-life, the *in situ*  $^{14}\text{C}$  ages should be affected more than the  $^{10}\text{Be}$  ages, and in both cases, the ages that we report may be treated as slightly minimum ages for deglaciation. The samples nearest the ice caps, in particular, were most likely to have been covered by relatively thick ice during the Little Ice Age. Yet, the  $^{10}\text{Be}$  ages from ice-sculpted bedrock samples adjacent to ice caps are not systematically younger than those  $^{10}\text{Be}$  ages from ice-sculpted bedrock samples farther away. For example, samples 05ORN-27 ( $8.7 \pm 0.5$  ka) and 05ORN-49 ( $8.2 \pm 0.9$  ka) are near present ice cap margins, whereas 06ORN-20 ( $7.7 \pm 0.5$  ka) lies beyond the vegetation trimline. Similarly, the short duration of ice cover during the Little Ice Age is well within the uncertainty of the *in situ*  $^{14}\text{C}$  ages, thus, it is not expected to have a statistically-significant influence on the ages. Indeed, sample 06ORN-16 ( $8.5 \pm 1.0$  ka), located in a valley below the vegetation trimline, is not statistically older than other many samples within the vegetation trimline.

There are, however, several *in situ*  $^{14}\text{C}$  ages that significantly post-date deglaciation. The youngest *in situ*  $^{14}\text{C}$  age (05SRP-72;  $2.2 \pm 0.4$  ka) is from a cobble atop a sandy kame feature and in a valley bottom below the vegetation trimline; we attribute this young age to either recent exhumation by frost processes or lab error. Four other samples, however, are from surfaces recently emerged from ice cap margins and are most easily explained by prolonged shielding by ice caps. These are 05ORN-4 ( $3.1 \pm 0.4$  ka), 05ORN-5 ( $3.3 \pm 0.4$  ka), 05ORN-32 ( $4.1 \pm 0.4$  ka) and 05SRP-15 ( $4.2 \pm 0.4$  ka), and their ages require more burial by ice than would have occurred only during the Little Ice Age (Fig. 7). Adding to the 750 yr of ice cover during the Little Ice Age (1250–2000 AD), the *in situ*  $^{14}\text{C}$  measurements require an additional  $\sim 1600$ – $2100$  yr of ice

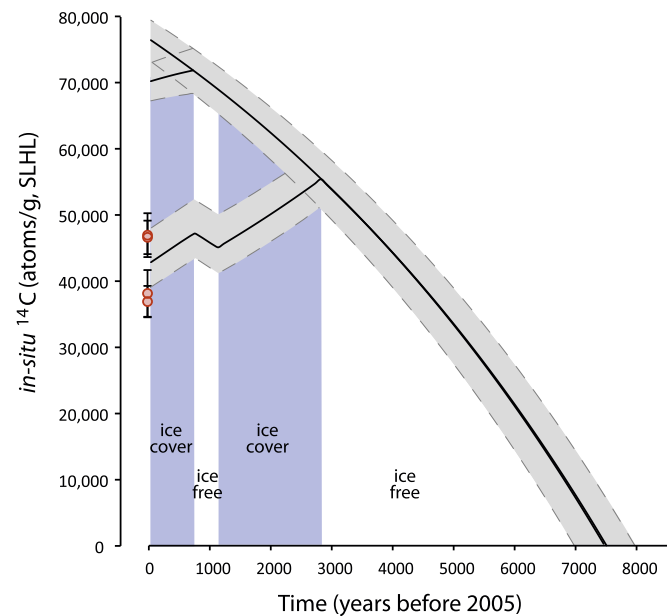


Fig. 7. Changes in the *in situ*  $^{14}\text{C}$  inventory through time starting with deglaciation at  $7.5 \pm 0.5$  ka. A simplistic scenario of ice cover during the Little Ice Age and from  $\sim 2.8$  to  $1.1$  ka generally explains the concentrations of four samples collected adjacent to ice cap margins in 2005 AD.

cover, and ~4650–5150 yr of ice free conditions since deglaciation (at ~7500 yr BP).

We use additional constraints on ice cap history presented in Anderson et al. (2008) to identify possible histories that explain the *in situ*  $^{14}\text{C}$  inventory in the four samples. Organic sediments in Chisel Lake, which lies well within the vegetation trimline and only ~500 m from the nearest ice cap, range from  $5.63 \pm 0.03$  cal ka to  $2.77 \pm 0.01$  cal ka, suggesting that the ice caps in the study area first grew ~2.80 cal ka (Anderson et al., 2008). Modeling *in situ*  $^{14}\text{C}$  accumulation beginning at deglaciation ( $7.6 \pm 1.5$  cal ka; see above) and burial by ice caps after ~2.8 cal ka generally explains the inventory in the four samples. However, no emerging vegetation from ice caps in the study area have ages (or “kill dates”) as old as 2800 cal yr BP; rather, most of the radiocarbon ages are ~1250 or ~1450 AD, suggesting an ice free period just prior to ice cap expansion at the beginning of the Little Ice Age (Anderson et al., 2008). Thus, it is likely that there was at least one ice free period between ~2800 cal yr BP and present, and this period may have been just prior to the Little Ice Age. This ice-free period cannot have lasted for more than a few centuries, otherwise the modeled *in situ*  $^{14}\text{C}$  inventory would be incompatible with the measured *in situ*  $^{14}\text{C}$  values. Furthermore, we acknowledge that there are samples very near extant ice cap margins that have *in situ*  $^{14}\text{C}$  ages showing no evidence of prolonged ice cap burial [e.g., 05TGR-25 ( $8.5 \pm 1.4$  ka) and 06ORN-6 ( $9.3 \pm 1.7$  ka)], suggesting that ice cap extent may not have been dramatically larger than at present, but probably configured differently. It is possible that as these ice caps grew throughout the late Holocene, their location was controlled not only by elevation, but also by snow patterns and wind drifting. If so, the location of ice cap margins during retreat does not necessarily reflect ice cap margins during their growth phase. In any case, most of the *in situ*  $^{14}\text{C}$  inventories are consistent with Neoglaciation beginning ~2800 cal yr BP at these elevations, after which ice caps have been mostly present, with at least one short period of ice cap recession prior to the Little Ice Age.

## 6. Conclusion

North-central Baffin Island contains a complex landscape that is the cumulative expression of successive occupations by polythermal ice sheets, expanding and retreating over dozens of glacial cycles. The presence/absence of inheritance can be used to characterize the geomorphic imprint of cold-bedded versus sliding conditions. The sharpness of the boundary between sliding and cold-bedded conditions on north-central Baffin Island and the pattern of cosmogenic nuclide inventories indicates that the zone of sliding ice migrated farther toward the ice source during the last glacial cycle than anytime in the past >1 Ma. Combined with previous work (e.g., Staiger et al., 2006; Refsnider and Miller, 2010), this suggests that as landscapes evolve, so does ice sheet behavior, supporting the notion that during this process some ice-sheet outlets are chosen over others (Kessler et al., 2008; Refsnider and Miller, 2010).

In landscapes that were occupied by polythermal ice sheets, cosmogenic-nuclide exposure dating with  $^{26}\text{Al}$  and  $^{10}\text{Be}$  is hampered by inheritance. In landscapes with pervasive inheritance, erratics can also have inheritance and can be a poor sample type for  $^{26}\text{Al}$  or  $^{10}\text{Be}$  dating. On the other hand, ice-sculpted bedrock has no inheritance in almost all cases, even at relatively high elevations. With the availability of *in situ*  $^{14}\text{C}$  and its relatively short half-life, we have another option for dating bedrock and erratics, in that no inheritance should exist in landscapes occupied by ice for more than 30 ky (i.e. the last glacial cycle). In our dataset, the average of the  $^{10}\text{Be}$  and *in situ*  $^{14}\text{C}$  ages overlap, and together provide an age for deglaciation of the north-central Baffin Island uplands.

*In situ*  $^{14}\text{C}$  also can be used to constrain ice-free versus ice-covered periods during the Holocene (Anderson et al., 2008; Goehring et al., 2011). Most of our samples collected adjacent to ice-cap margins in 2005 AD have too little *in situ*  $^{14}\text{C}$  to be explained by a simple history of exposure since deglaciation followed by burial during the Little Ice Age. Assuming deglaciation took place ~7500 yr ago, then their  $^{14}\text{C}$  inventories indicate that ice caps were smaller than they are today for roughly 60% of the time. Used in this manner, *in situ*  $^{14}\text{C}$  has the potential to constrain spatial patterns of ice-free versus Neoglaciation conditions during the Holocene in glaciated regions throughout the globe. Furthermore, when combined with other chronological information (e.g., vegetation kill dates, reworked logs, lake sediment records, historical observations), *in situ*  $^{14}\text{C}$  inventories can be used to produce well-constrained histories of Neoglaciation. Finally, many elements of landscape history can be deciphered using multiple cosmogenic isotopes, even in landscapes that are the product of polythermal ice-sheet occupation and thus pose significant challenges to single-nuclide cosmogenic nuclide exposure dating.

## Acknowledgments

This work was supported by the National Science Foundation Office of Polar Programs grant ARC-0454601. BaffinLand Mines provided essential logistical assistance; we thank CHM2Hill Polar Field Services for additional logistical support. Jamesee Qillaq, Steven Tagak and Dale Hess provided field assistance; Lena Håkansson and Nicolás Young provided assistance in the laboratory; Stephen DeVogel helped with figures. We also thank Tim Jull, Rich Cruz, and Dana Biddulph of the Arizona AMS facility for *in situ*  $^{14}\text{C}$  analyses. Finally, we thank two anonymous reviewers for providing critical comments on this manuscript.

Editorial handling by: N. Akçar

## Appendix A. Supplementary data

Supplementary data related to this article can be found at <http://dx.doi.org/10.1016/j.quageo.2012.11.005>.

## References

- Anderson, R.K., Miller, G.H., Briner, J.P., Lifton, N.A., DeVogel, S.B., 2008. A millennial perspective on Arctic warming from  $^{14}\text{C}$  in quartz and plants emerging beneath ice caps. *Geophysical Research Letters* 35, L01502.
- Andrews, J.T., Ives, J.D., 1978. “Cockburn” nomenclature and the Late Quaternary history of the eastern Canadian Arctic. *Arctic Alpine Research* 10, 617–633.
- Andrews, J.T., Barnett, D.M., 1979. Holocene (Neoglaciation) moraine and proglacial lake chronology, Barnes ice cap, Canada. *Boreas* 8, 341–358.
- Andrews, J.T., Davis, P.T., Locke, C., 1976. Little ice age permanent snowcover in the eastern Canadian Arctic – extent mapped from Landsat-1 satellite imagery. *Geografiska Annaler* 58A, 71–81.
- Andrews, J.T., Stravers, J.A., Miller, G.H., 1985. Patterns of glacial erosion and deposition around Cumberland Sound, Frobisher Bay and Hudson Strait, and the location of ice streams in the eastern Canadian Arctic. In: Woldenburg, M.J. (Ed.), *Models in Geomorphology*. Allen & Unwin, London, pp. 93–117.
- Balco, G., 2011. Contributions and unrealized potential contributions of cosmogenic-nuclide exposure dating to glacier chronology, 1990–2010. *Quaternary Science Reviews* 30, 3–27.
- Balco, G., Stone, J.O., Lifton, N.A., Dunai, T.J., 2008. A complete and easily accessible means of calculating surface exposure ages or erosion rates from  $^{10}\text{Be}$  and  $^{26}\text{Al}$  measurements. *Quaternary Geochronology* 3, 174–195.
- Balco, G., Briner, J.P., Finkel, R.C., Rayburn, J.A., Ridge, J.C., Schaefer, J.M., 2009. Regional beryllium-10 production rate calibration for late-glacial northeastern North America. *Quaternary Geochronology* 4, 93–107.
- Bierman, P.R., Marsella, K.A., Patterson, C., Thompson Davis, T., Caffee, M., 1999. Mid-Pleistocene cosmogenic minimum-age limits for pre-Wisconsin glacial surfaces in southwestern Minnesota and southern Baffin Island: a multiple nuclide approach. *Geomorphology* 27, 25–39.
- Briner, J.P., Miller, G.H., Davis, P.T., Bierman, P.R., Caffee, M., 2003. Last glacial maximum ice sheet dynamics in Arctic Canada inferred from young erratics perched on ancient tors. *Quaternary Science Reviews* 22, 437–444.

- Briner, J.P., Miller, G.H., Davis, P.T., Finkel, R.C., 2005. Cosmogenic exposure dating in arctic glacial landscapes: implications for the glacial history of northeastern Baffin Island, Arctic Canada. *Canadian Journal of Earth Sciences* 42, 67–84.
- Briner, J.P., Miller, G.H., Thompson Davis, P., Finkel, R.C., 2006. Cosmogenic radionuclides from fiord landscapes support differential erosion by overriding ice sheets. *Geological Society of America Bulletin* 118, 406–420.
- Briner, J.P., Overeem, I., Miller, G.H., Finkel, R., 2007. The deglaciation of Clyde Inlet, northeastern Baffin Island, Arctic Canada. *Journal of Quaternary Science* 22, 223–232.
- Briner, J.P., Miller, G.H., Finkel, R., Hess, D.P., 2008. Glacial erosion at the fiord onset zone and implications for the organization of ice flow on Baffin Island. *Geomorphology* 97, 126–134.
- Briner, J.P., Bini, A.C., Anderson, R.S., 2009. Rapid early Holocene retreat of a Laurentide outlet glacier through an Arctic fiord. *Nature Geoscience* 2, 496–499.
- Brook, E.J., Kurz, M.D., Ackert, R.P., Denton, G.H., Brown, E.T., Raisbeck, G.M., Yiou, F., 1993. Chronology of Taylor Glacier advances in Arena Valley, Antarctica using *in situ* cosmogenic  $^3\text{He}$  and  $^{10}\text{Be}$ . *Quaternary Research* 39, 11–23.
- Brook, E.J., Nesje, A., Lehman, S.J., Raisbeck, G.M., Yiou, F., 1996. Cosmogenic nuclide exposure ages along a vertical transect in western Norway: implications for the height of the Fennoscandian ice sheet. *Geology* 24, 207–210.
- De Angelis, H., Kleman, J., 2007. Palaeo-ice streams in the Foxe/Baffin sector of the Laurentide Ice sheet. *Quaternary Science Reviews* 26, 1313–1331.
- Dugan, B., 2008. New production rate estimates for *in situ* cosmogenic  $^{14}\text{C}$  from Lake Bonneville, Utah, and northwestern Scotland, M.S. thesis, Tucson, AZ, 46 p.
- Dredge, L.A., 2004. Till Geochemistry Results, Central Baffin Island, Nunavut (NTS 37A, 37D, 27B, 27C). Open File 4543. Geological Survey of Canada, Ottawa.
- Dyke, A.S., 2008. The Steensby Inlet Ice Stream in the context of the deglaciation of northern Baffin Island, eastern Canadian Arctic. *Earth Surface Processes and Landforms* 33, 573–592.
- Dyke, A., Moore, A., Robertson, L., 2003. Deglaciation of North America. Geological Survey of Canada Open File Report 1574, Natural Resources Canada, Ottawa, Ontario.
- Fabel, D., Harbor, J., 1999. The use of *in situ* produced cosmogenic radionuclides in glaciology and glacial geomorphology. *Annals of Glaciology* 29, 103–110.
- Fabel, D., Stroeven, A.P., Harbor, J., Kleman, J., Elmore, D., Fink, D., 2002. Landscape preservation under Fennoscandian ice sheets determined from *in situ* produced Be-10 and Al-26. *Earth and Planetary Science Letters* 201, 397–406.
- Falconer, G., 1966. Preservation of vegetation and patterned ground under a thin ice body in northern Baffin Island, N.W.T. *Geographical Bulletin* 8, 194–200.
- Goehring, B.M., Brook, E.J., Linge, H., Raisbeck, G.M., Yiou, F., 2008. Beryllium-10 exposure ages of erratic boulders in southern Norway and implications for the history of the Fennoscandian Ice Sheet. *Quaternary Science Reviews* 27, 320–326.
- Goehring, B.M., Schaefer, J.M., Schluechter, C., Lifton, N., Finkel, R.C., Timothy Jull, A.J., Akcar, N., Alley, R., 2011. The Rhone Glacier was smaller than today for most of the Holocene. *Geology* 39, 679–682.
- Häkansson, L., Briner, J.P., Alexanderson, H., Aldahan, A., Possnert, G., 2007.  $^{10}\text{Be}$  ages from coastal northeast Greenland constrain the extent of the Greenland Ice Sheet during the Last Glacial Maximum. *Quaternary Science Reviews* 26, 2316–2321.
- Harbor, J., Stroeven, A.P., Fabel, D., Clarhäll, A., Kleman, J., Li, Y., Elmore, D., Fink, D., 2006. Cosmogenic nuclide evidence for minimal erosion across two subglacial sliding boundaries of the late glacial Fennoscandian ice sheet. *Geomorphology* 75, 90–99.
- Hippe, K., Kober, F., Wacker, L., Fahrni, S., Ivy-Ochs, S., Akcar, N., Schluchter, C., Wieler, R., 2013. An update on cosmogenic *in situ*  $^{14}\text{C}$  analysis at Zürich. *Nuclear Instruments and Methods B* 294, 81–86.
- Heisinger, B., Lal, D., Jull, A., Kubik, P., Ivy-Ochs, S., Neumaier, S., Knie, K., Lazarev, V., Nolte, E., 2002a. Production of selected cosmogenic radionuclides by muons 1. Fast muons. *Earth and Planetary Science Letters* 200, 345–355.
- Heisinger, B., Lal, D., Jull, A., Kubik, P., Ivy-Ochs, S., Knie, K., Nolte, E., 2002b. Production of selected cosmogenic radionuclides by muons: 2. Capture of negative muons. *Earth and Planetary Science Letters* 200, 357–369.
- Ives, J.D., 1962. Indications of recent extensive glacierization in north-central Baffin Island. *Journal of Glaciology* 4, 197–205.
- Ives, J.D., Andrews, J.T., 1963. Studies in the physical geography of north-central Baffin Island. N. W.T. *Geographical Bulletin* 19, 5–48.
- Kaplan, M.R., Miller, G.H., Steig, E.J., 2001. Low-gradient outlet glaciers (ice streams?) drained the Laurentide ice sheet. *Geology* 29, 343–346.
- Kessler, M.A., Anderson, R.S., Briner, J.P., 2008. Fjord insertion into continental margins driven by topographic steering of ice. *Nature Geoscience* 1, 365–369.
- Kleman, J., 1994. Preservation of landforms under ice sheets and ice caps. *Geomorphology* 9, 19–32.
- Kleman, J., Stroeven, A.P., 1997. Preglacial surface remnants and quaternary glacial regimes in northwest Sweden. *Geomorphology* 19, 35–54.
- Kleman, J., Hättestrand, C., 1999. Frozen-bed Fennoscandian and Laurentide ice sheets during the Last Glacial maximum. *Nature* 402, 63–66.
- Kleman, J., Stroeven, A.P., Lundqvist, J., 2008. Patterns of quaternary ice sheet erosion and deposition in Fennoscandia and a theoretical framework for explanation. *Geomorphology* 97, 73–90.
- Kohl, C.P., Nishizumi, K., 1992. Chemical isolation of quartz for measurement of *in situ*-produced cosmogenic nuclides. *Geochimica et Cosmochimica Acta* 56, 3583–3587.
- Li, Y., Fabel, D., Stroeven, A.P., Harbor, J., 2008. Unraveling complex exposure-burial histories of bedrock surfaces under ice sheets by integrating cosmogenic nuclide concentrations with climate proxy records. *Geomorphology* 99, 139–149.
- Lifton, N.A., Timothy Jull, A.J., Quade, J.A., 2001. A new extraction technique and production rate estimate for *in situ* cosmogenic  $^{14}\text{C}$  in quartz. *Geochimica et Cosmochimica Acta* 65, 1953–1969.
- Little, E.C., Holme, P., Hilchey, A., Young, M., 2004. Glacial Geology, Ice-movement Chronology and Drift Prospecting in the Vicinity of Icebound Lakes (NTS 37G), Northern Baffin Island, Nunavut. Geological Survey of Canada Current Research No. 2004–B1.
- Locke, C.W., Locke III, W.W., 1977. Little Ice Age snow-cover extent and paleoglaciation thresholds: north-central Baffin Island, N.W.T. Canada. *Arctic and Alpine Research* 9, 291–300.
- Marquette, G.C., Gray, J.T., Gosse, J.C., Courchesne, F., Stockli, L., Macpherson, G., Finkel, R., 2004. Felsenmeer persistence under nonerosive nonerosive ice in the Torngat and Kaumajet Mountains, Quebec and Labrador, as determined by soil weathering and cosmogenic nuclide exposure dating. *Canadian Journal of Earth Sciences* 41, 19–38.
- Marsella, K.A., Bierman, P.R., Davis, P.T., Caffee, M.W., 2000. Cosmogenic  $^{10}\text{Be}$  and  $^{26}\text{Al}$  ages for the Last Glacial Maximum, eastern Baffin Island, Arctic Canada. *Geological Society of America* 112, 1296–1312.
- McNeely, R., Brennan, J., 2005. Geological Survey of Canada Revised Shell Dates. Geological Survey of Canada. Open File 5019.
- Miller, G.H., Wolfe, A.P., Steig, E.J., Sauer, P.E., Kaplan, M.R., Briner, J.P., 2002. The Goldilocks dilemma: big ice, little ice, or “just-right” ice in the eastern Canadian Arctic. *Quaternary Science Reviews* 21, 33–48.
- Miller, G., Briner, J., Lifton, N., Finkel, R., 2006. Limited ice-sheet erosion and complex exposure histories derived from *in situ* cosmogenic  $^{10}\text{Be}$ ,  $^{26}\text{Al}$ , and  $^{14}\text{C}$  on Baffin Island, Arctic Canada. *Quaternary Geochronology* 1, 74–85.
- Miller, G.H., Geirsdóttir, Á., Zhong, Y., Larsen, D.J., Otto-Bliensner, B.L., Holland, M.M., Baily, D.A., Refsnider, K.A., Lehman, S.J., Southon, J.R., Anderson, C., Björnsson, H., Thordarson, T., 2012. Abrupt onset of the Little Ice Age triggered by volcanism and sustained by sea-ice/ocean feedbacks. *Geophysical Research Letters* 39, L02708.
- Nishizumi, K., 2004. Preparation of  $^{26}\text{Al}$  AMS standards. *Nuclear Instruments and Methods in Physics Research Section B, Beam Interactions with Materials and Atoms* 223–224, 388–392.
- Nishizumi, K., Imamura, M., Caffee, M., Southon, J., Finkel, R., McAnich, J., 2007. Absolute calibration of  $^{10}\text{Be}$  AMS standards. *Nuclear Instruments and Methods in Physics Research B* 258, 403–413.
- Pigati, J.S., 2004. Experimental developments and application of carbon-14 and *in situ* cosmogenic nuclide dating techniques, Ph.D. thesis, Univ. of Ariz., Tucson.
- Refsnider, K.A., Miller, G.H., 2010. Reorganization of ice sheet flow patterns in Arctic Canada and the mid-Pleistocene transition. *Geophysical Research Letters* 37, L13502. <http://dx.doi.org/10.1029/2010GL043478>.
- Staiger, J.W., Gosse, J., Little, E.C., Utting, D.J., Finkel, R., Johnson, J.V., Fastook, J., 2006. Glacial erosion and sediment dispersion from detrital cosmogenic nuclide analysis of till. *Quaternary Geochronology* 1, 29–42.
- Steig, E.J., Wolfe, A.P., Miller, G.H., 1998. Wisconsinan refugia and the glacial history of eastern Baffin Island, Arctic Canada: coupled evidence from cosmogenic isotopes and lake sediments. *Geology* 26, 835–838.
- Stone, J.O., Balco, G.A., Sugden, D.E., Caffee, M.W., Sass III, L.C., Cowdery, S.G., Siddoway, C., 2003. Holocene deglaciation of Marie Byrd Land, West Antarctica. *Science* 299, 99–102.
- Stroeven, A.P., Fabel, D., Hättestrand, C., Harbor, J., 2002. A relict landscape in the centre of Fennoscandian glaciation: cosmogenic radionuclide evidence of tors preserved through multiple glacial cycles. *Geomorphology* 44, 145–154.
- Stroeven, A.P., Fabel, D., Harbor, J.M., Fink, D., Caffee, M.W., Dahlgren, T., 2011. Importance of sampling across an assemblage of glacial landforms for interpreting cosmogenic ages of deglaciation. *Quaternary Research* 76, 148–156.
- Sugden, D., 1978. Glacial erosion by the Laurentide ice sheet. *Journal of Glaciology* 20, 367–391.
- Sugden, D.E., Balco, G., Cowdery, S.G., Stone, J.O., Sass, L.C., 2005. Selective glacial erosion and weathering zones in the coastal mountains of Marie Byrd Land, Antarctica. *Geomorphology* 67, 317–334.
- Utting, D.J., Little, E.C., Young, M.D., McCurdy, M.W., Dyke, A.S., Girard, I., 2008. Till, Stream-sediment and Bedrock Analyses, North Baffin Island, Nunavut (NTS 37E, F, G, H and 47E). Open File 5742, Geological Survey of Canada, Ottawa.
- Williams, L.D., 1978. The little ice age glaciation level on Baffin Island, Arctic Canada. *Palaogeography, Palaeoclimatology, Palaeoecology* 25, 199–207.